JGR Oceans

RESEARCH ARTICLE
10.1029/2023JC019630

Mechanisms of Salt Overspill at Estuarine Network Junctions Explained With an Idealized Model

Bouke Biemond[1], Huib E. de Swart[1], and Henk A. Dijkstra[1]

[1]Department of Physics, Institute for Marine and Atmospheric research Utrecht, Utrecht University, Utrecht, The Netherlands

Key Points:

- Dependence of salt overspill is quantified in case of a simple network for different river discharges, tidal strengths, and geometries
- Values of overspill calculated with an idealized model are well approximated by an analytical expression derived from basic physics
- Salt overspill strongly depends on the net water transport in the network and on the differential salt import in the channels

Supporting Information:

Supporting Information may be found in the online version of this article.

Correspondence to:

B. Biemond,
w.t.biemond@uu.nl

Citation:

Biemond, B., de Swart, H. E., & Dijkstra, H. A. (2023). Mechanisms of salt overspill at estuarine network junctions explained with an idealized model. *Journal of Geophysical Research: Oceans*, *128*, e2023JC019630. https://doi.org/10.1029/2023JC019630

Received 4 JAN 2023
Accepted 7 MAR 2023

Abstract Salt overspill, defined as the net salt transport from a channel of an estuarine network through a junction to another channel, can be a major contributor to salt intrusion. Here, an idealized subtidal model is constructed of a network consisting of one river channel and two sea channels, and used to investigate the sensitivity of overspill to different values of river discharge, tidal current, width, and depth of the channels. Two prototype systems are considered: the North and South Passage of the Yangtze Estuary and the Modaomen and Hongwan Channel of the Pearl River Estuary. Model results indicate that in both systems, increasing river discharge decreases the amount of salt overspill, except in the regime of weak river discharge in the Yangtze Estuary. Increasing the strength of the tidal current increases the overspill in the Yangtze Estuary, but it decreases the overspill in the Modaomen Estuary. Analysis of the model results shows that salt overspill is linearly related to the salinity difference at the upstream boundary of the two seaward channels, when they are considered as single channel estuaries. This salinity difference occurs because conditions in the channels are not identical, which results in different net water transports (causing export of salt), exchange flows, and horizontal diffusion (causing import of salt). An analytical expression is derived, which explains the dependency of salt overspill to the factors mentioned above.

Plain Language Summary Estuarine deltas are areas where a river splits into multiple channels, such that it has several outflows to the sea. These regions are susceptible to salt intrusion: salty sea water intruding into the estuarine delta, which may for example hamper intake of fresh water. Specifically, we investigate the process of salt transport from one channel to another channel through a single junction in an estuarine delta. This salt transport is called salt overspill. Two estuarine deltas are taken as examples: part of the Yangtze Estuary and the Modaomen Estuary. We study why overspill happens in these systems and assess the sensitivity of overspill to river discharge, tidal strength, and changes of the geometry of the channels. We find that, because salt intrusion in the separate channels responds differently to these factors, the salt overspill also strongly depends on them. More specifically, we show that in the Yangtze Estuary salt is transported from the South Passage into the North Passage, because the South Passage is much wider than the North Passage. In the Modaomen Estuary, salt flows from the Hongwan Channel into the Modaomen Channel, because the Hongwan Channel only receives little fresh water from the Modaomen Waterway.

1. Introduction

Estuarine deltas are among the most heavily populated places on earth. Fertile grounds and opportunities for transport over water provide economic advantages in these regions. This has resulted in a number of megacities built in estuarine deltas, for example at the east coasts of China and Bangladesh and in the western Netherlands. The high population density in these areas generates increasing pressure on the natural functioning of an estuarine delta (see e.g., Eslami et al., 2021). Fresh water in the estuary is often used for irrigation, industry, and drinking water. However, all these activities result in enhanced salt water intrusion, thereby causing for example loss of vegetation and reducing the productivity of agricultural lands.

Salt water intrusion in a one-channel estuary has been extensively studied and theoretical frameworks exist which explain the properties of the salt water intrusion in different estuaries (Dijkstra & Schuttelaars, 2021; Geyer & MacCready, 2014; Hansen & Rattray, 1966, and references therein). The extent of the salt intrusion is determined by the competition between river flow transporting salt downstream and several processes transporting salt upstream, such as density-driven flow and tidal pumping.

However, an estuarine delta consists of a network of interconnected channels. Salt intrusion in such a system is more complicated than in a single channel, as the distribution of salt and fresh water over the channels are

additional unknowns. In this study, the focus will be on the process of salt overspill, here defined as the net salt transport from one channel through a junction into another. This overspill may have an important effect on salt intrusion in deltas, and makes it more difficult to manage this.

Observed salt overspill in two estuarine deltas with a relatively simple geometry form the motivation for this study. The first case concerns overspill that occurs at the junction of the South Channel, South Passage, and North Passage of the Yangtze Estuary, located at the east coast of China (Figure 1a). As in many estuaries, major modifications have been implemented in this estuary: far upstream, the Three Gorges Dam in the Yangtze River stores significant amounts of water and thus changes the discharge reaching the estuary (Gao et al., 2013). Within the Deep Waterway Project, the North Passage was deepened and narrowed to make the harbor of Shanghai more accessible. These alterations of the geometry of the channel led to changes to the freshwater transport and salt intrusion in the estuary (Hu & Ding, 2009; J. Zhu et al., 2006). J. Zhu et al. (2018) mention that salt intrusion in the South Passage is stronger than in the North Passage, indicating that there is overspill from the South Passage to the North Passage. However, the sensitivity of overspill to physical forcing and changes to the channel geometry has not been assessed. The second case considered concerns overspill that occurs at the junction of Modaomen Waterway, the Hongwan Channel, and the Modaomen Channel in the Pearl River Estuary in South-East China (Figure 1b). The direction of the salt transport at this junction is debated in the literature. While the model studies of Gong et al. (2012) and B. Wang et al. (2012) indicate that the Hongwan Waterway is an important source of salt for the Modaomen Waterway, Gong et al. (2014) state that, based on observations, "the Hongwan Waterway is not a salt source to the mainstem in the study period." Since the physical forcing conditions of estuaries are strongly time dependent, mostly due to changes in river discharge and the spring-neap cycle of the tides, a possible explanation of these contradictory results is that the direction of the overspill depends on the forcing conditions. This is indeed noted by Gong et al. (2014), but a framework that explains how the overspill depends on forcing conditions is lacking. Furthermore, it is important to gain more insight into the effects of anthropogenic measures, such as land reclamation, as the latter is known to have impact on salt intrusion (Liu et al., 2019).

This study aims at gaining more fundamental knowledge of salt overspill at channel junctions and to better understand salt intrusion in an estuarine network. The Yangtze and Modaomen are considered as prototype estuaries, but the results will also be useful to understand the dynamics of other estuarine networks. From this aim, three objectives are specified: (a) Understand and quantify the direction and magnitude of salt overspill from the basic physics. (b) Understand and quantify the dependence of salt overspill on river discharge and tidal strength. (c) Understand and quantify the dependence of salt overspill on the channel width and depth. To determine the underlying mechanisms, an idealized model will be employed. A spatially one-dimensional model is not appropriate for this problem, as the vertical structure of currents and salinity are an essential part of estuarine dynamics. Motivated by the success of width-averaged (or 2DV) models for single channels (see e.g., Dijkstra & Schuttelaars, 2021; MacCready, 2004, 2007; Ralston et al., 2008), this type of model will be used.

The remainder of this article is organized as follows. In Section 2 the idealized model is described, which extends the model of Biemond et al. (2022) to a channel network. In Section 3.1, model results for reference simulations

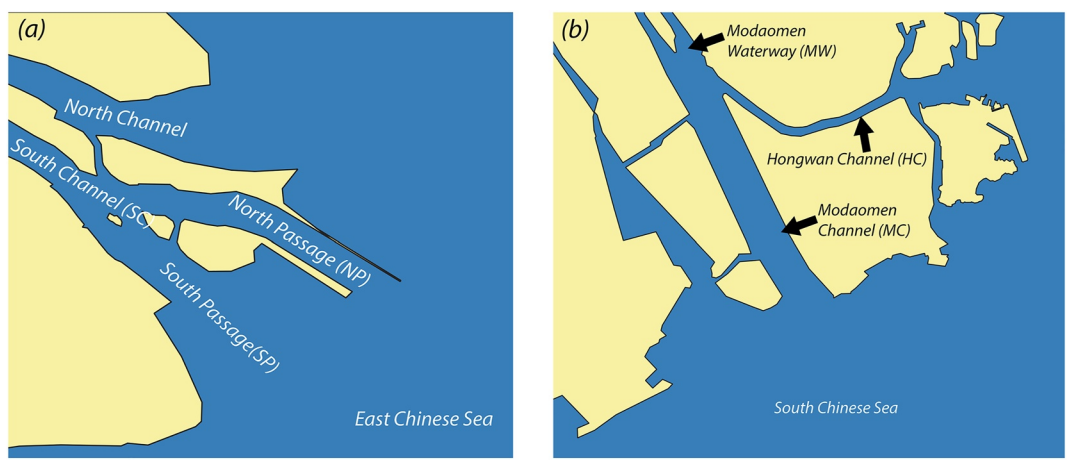

Figure 1. (a) Geometry of (part of) the Yangtze Estuary. (b) Geometry of the Modaomen Estuary.

are presented and an equation for overspill is derived from the basic physics. Section 3.2 contains results for the sensitivity of the overspill to river discharge and tidal strength, and Section 3.3 presents results regarding the sensitivity of overspill to the width and depth of the channels. The results are discussed in Section 4 and conclusions are given in Section 5.

2. Material and Methods

2.1. Model Formulation

To study the underlying mechanisms of salt overspill, a width-averaged model in a simple channel network is used. As is illustrated in Figure 2a, it consists of three channels, where the first (labeled Channel 1) is connected to the river and the junction. This channel splits at the junction in two channels, labeled Channels 2 and 3, that are connected to the sea. These channels consist of an estuarine section, between the junction and the estuary mouth, and a strongly converging adjacent sea section, from the mouth to the open ocean (indicated with dashed lines in Figure 2), which serves as a simple representation of the region of freshwater influence.

The channels have a length L_j and a constant depth H_j, where the subscript $j = 1, 2, 3$ indicates the channel index. The length of the adjacent sea sections is $L_{\text{sea},j}$. The horizontal coordinate in the estuarine channels in the network is indicated with x_j, which runs from $x_j = -L_j$ (the upstream boundary) to $x_j = 0$ (the downstream boundary). In the adjacent sea sections x_j runs from $x_j = 0$ (the estuary mouth) to $x_j = L_{\text{sea},j}$ (the ocean boundary). Hereafter, channel indices will be omitted for readability if the equation holds for all channels.

The width b (see Figure 2b) is described by the exponential function

$$b(x) = b_u \exp\left(\frac{x+L}{L_b}\right) \quad \text{with} \quad L_b = \begin{cases} \dfrac{L}{\log\left(\dfrac{b_d}{b_u}\right)}, & \text{for } -L < x < 0, \\ L_{b,sea}, & \text{for } 0 < x < L_{sea}, \end{cases} \tag{1}$$

where b_u is the width at the upstream limit of the channel, L_b is the width convergence length, and b_d is the width at the downstream limit of the estuarine channel. Note that the width is continuous at the mouths, but not necessarily at the junction. Channel 1 has no adjacent sea part, so only the formulation for $x < 0$ is used.

2.1.1. Hydrodynamic and Salinity Module

The width-averaged model presented here builds on that in Biemond et al. (2022), which is an extension of the model developed by MacCready (2004). Following many earlier studies (Geyer & MacCready, 2014 and references therein), subtidal water motion in each channel is considered and the Boussinesq and hydrostatic approximations are assumed to hold. The steady state horizontal velocity component u is determined by a momentum balance between a barotropic and baroclinic pressure gradient force and the internal frictional force; the vertical velocity w is determined by continuity:

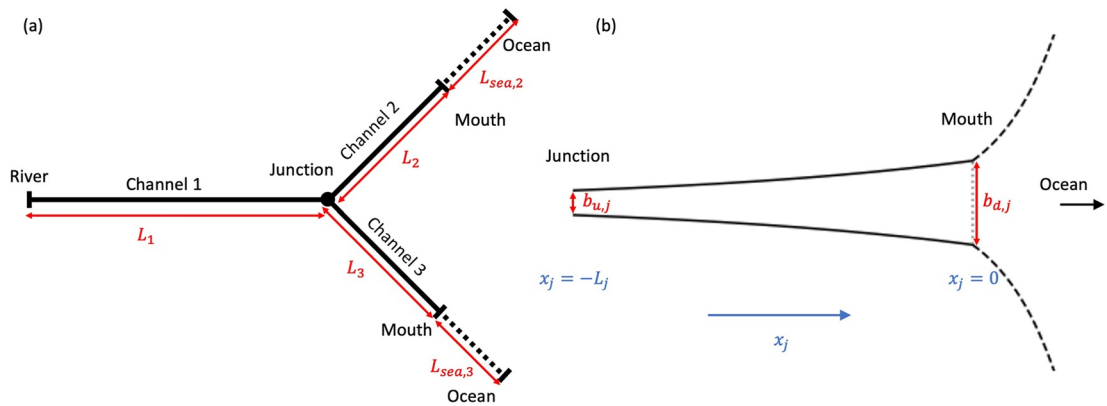

Figure 2. (a) A sketch of the domain used in the model. (b) A sketch of the local situation in a channel seawards of the junction. The channel landwards of the junction is similar, except there is no adjacent sea section.

$$0 = -g\frac{\partial \eta}{\partial x} - g\beta \int_z^0 \frac{\partial s}{\partial x} dz' + \frac{\partial}{\partial z}\left(A_v \frac{\partial u}{\partial z}\right), \tag{2}$$

$$\frac{\partial (bu)}{\partial x} + \frac{\partial (bw)}{\partial z} = 0. \tag{3}$$

In these equations, x and z are horizontal and vertical coordinates, $g = 9.81$ m s^{-2} is gravitational acceleration, η is sea surface height, $\beta = 7.6 \times 10^{-4}$ (g/kg)$^{-1}$ is the isohaline contraction coefficient, s is absolute salinity (in g/kg), and A_v is the constant vertical viscosity coefficient. At the surface, a zero stress condition is assumed (no wind) and at the bottom and surface kinematic boundary conditions are used. At the bed, a linearized partial slip condition is employed, which reads

$$A_v \frac{\partial u}{\partial z} = S_f u, \tag{4}$$

where $S_f = \frac{2A_v}{H}$ is the friction coefficient. The velocity components u and w can then be expressed as follows (see Supporting Information S1 for the full derivation):

$$u = \bar{u}\left(\frac{6}{5} - \frac{3}{5}\frac{z^2}{H^2}\right) + \alpha \frac{d\bar{s}}{dx}\left(\frac{8}{5} - \frac{54}{5}\frac{z^2}{H^2} - 8\frac{z^3}{H^3}\right), \tag{5a}$$

$$w = \alpha H\left(\frac{d^2\bar{s}}{dx^2} + L_b^{-1}\frac{d\bar{s}}{dx}\right)\left(2\frac{z^4}{H^4} + \frac{18}{5}\frac{z^3}{H^3} - \frac{8}{5}\frac{z}{H}\right). \tag{5b}$$

Here, a bar denotes an average over the depth, and $\bar{u} = \frac{Q}{bH}$. The quantity Q is the net water transport in the channel and is to be determined by conditions at the river head, estuary mouths, and at the junctions (Section 2.1.2). Also, $\alpha = \frac{g\beta H^3}{48A_v}$ is a coefficient determining the strength of the exchange flow, which is the current induced by the horizontal density gradient in the system.

Mass conservation of salt yields the following width-averaged steady advection-diffusion equation for salinity:

$$\frac{1}{b}\frac{\partial}{\partial x}\left(bus - bK_h\frac{\partial s}{\partial x}\right) + \frac{\partial}{\partial z}\left(ws - K_v\frac{\partial s}{\partial z}\right) = 0, \tag{6}$$

in which K_h and K_v are the (subtidal, turbulent) constant horizontal and vertical diffusivity coefficients, respectively. The parametrizations of the viscosity and diffusivity coefficients read

$$A_v = c_v U_T H, \quad K_v = \frac{A_v}{S_c}, \quad K_h = c_h\left(\frac{T_{tide}}{4}U_T\right)U_T, \tag{7}$$

with $c_v = 7.28 \cdot 10^{-5}$ being a calibration constant, U_T the amplitude of the tidal current (which is an input parameter in this model), and $S_c = 2.2$ the Schmidt number. In the expression for K_h, $T_{tide} = 12.42$ hr is the period of the M_2 tide and $c_h = 0.0224$ is a dimensionless constant. These parametrizations are taken from MacCready (2004) and Ralston et al. (2008). In the adjacent sea domain, $K_h = K_h|_{\text{mouth}} \exp\left(\frac{x}{L_b}\right)$, to account for the increase of the magnitude of horizontal diffusion in the open sea.

2.1.2. Conditions at the Boundaries and Junctions

To complete the model for the network (Figure 2), boundary conditions have to be specified at the river head, the two sea boundaries, and at the junction. At the river head

$$Q_1 = Q_{riv}, \quad s = 0, \tag{8}$$

where Q_{riv} is a prescribed river discharge. In order to guarantee that the salt transport through the river boundary is negligible, L_1 is chosen such that there is sufficient distance between the river head and the limit of salt intrusion.

At the ocean boundary we prescribe

$$\eta_j = \eta_{oc,j}, \quad s_j = s_{oc}, \tag{9}$$

in which $j = 2, 3$ are channel indices, η_{oc} is the tidally mean water level at the ocean boundary, and s_{oc} is a prescribed constant ocean salinity. This condition assumes that the ocean boundaries are located outside the region of freshwater influence.

At the junction, we impose.

$$\eta_1 = \eta_2 = \eta_3, \tag{10a}$$

$$Q_1 = Q_2 + Q_3, \tag{10b}$$

$$s_1\left(\frac{z_1}{H_1}\right) = s_2\left(\frac{z_2}{H_2}\right) = s_3\left(\frac{z_3}{H_3}\right), \tag{10c}$$

$$b_{d,1}\, H_1\left(u_1 s_1 - K_{h,1}\frac{\partial s_1}{\partial x_1}\right) = b_{u,2}\, H_2\left(u_2 s_2 - K_{h,2}\frac{\partial s_2}{\partial x_2}\right) + b_{u,3}\, H_3\left(u_s s_3 \text{-} K_{h,3}\frac{\partial s_3}{\partial x_3}\right), \tag{10d}$$

where $b_{u,j}$ and $b_{d,j}$ indicate the upstream and downstream width of channel j, respectively (see Equation 1). The first condition expresses the requirement that water level should be continuous at the junction and the second condition represents conservation of volume (J. Wang et al., 2021). The third condition is continuity of salinity, and the last equation indicates that the salt flux divides over the different channels. At the boundary between the estuarine channel and the adjacent sea domain, we apply the same conditions, but here only for two channels.

2.1.3. Solution Procedure

First, the discharges in Channel 2 and Channel 3 are calculated. Water level is related to discharge according to (from integrating Equation 2 twice over z and application of the boundary conditions, see Supporting Information S1)

$$\frac{\partial \eta}{\partial x} = -\frac{9}{20}\beta H\frac{\partial \bar{s}}{\partial x} - \frac{6}{5}\frac{A_v Q}{gbH^3}, \tag{11}$$

where, similarly as in Equation 5, $\bar{s}$ is the depth-averaged salinity. We now make the assumption that the water setup due to salinity is balanced by a water level difference between the mouths of the channels, and thus does not play a role in the water distribution, so the water setup is governed by internal friction. The motivation for doing this is that, as will appear later on, it leads to model results that compare well with field data. The implications and validity of this assumption will be discussed in more detail in Section 4. An additional advantage of this assumption is that it allows for finding analytical expressions for the net water transport in each channel, which read

$$Q_2 = \frac{\frac{5}{6}g(\eta_{oc,2} - \eta_{oc,3}) + \frac{A_{v,2}}{H_2^3}\int_{-L_2}^{0} b_2^{-1}\, dx\; Q_1}{\frac{A_{v,2}}{H_2^3}\int_{-L_2}^{0} b_2^{-1}\, dx + \frac{A_{v,3}}{H_3^3}\int_{-L_3}^{0} b_3^{-1}\, dx}, \quad Q_3 = Q_1 - Q_2. \tag{12}$$

Note that the geometry and water level of Channel 1 do not affect the water distribution. When the net water transports are known, the analytical expressions for the velocities are substituted in the salt balance Equation 6, and this equation is solved numerically for s. The solution procedure is outlined in Supporting Information S1. In summary, a Galerkin method is used in the vertical, while in the horizontal central differences are used. This gives a coupled system of algebraic equations which is solved with the Newton-Raphson algorithm.

2.2. Overspill Diagnostics

The horizontal net salt transport T in each channel reads

$$T = b\int_{-H}^{0}\left(us - K_h\frac{\partial s}{\partial x}\right)dz = \underbrace{Q\bar{s}}_{T_Q} + \underbrace{bH\overline{u's'}}_{T_E} - \underbrace{bHK_h\frac{\partial \bar{s}}{\partial x}}_{T_D}, \tag{13}$$

Table 1
Geometrical Properties of the Different Channels, Where b_u and b_d Are the Width at the Upstream and Downstream Limit of the Channels, Respectively, and the Width of These Channels Is Varied According to Equation 1

Yangtze Estuary	South Channel	South Passage	North Passage
L [km]	200	54	61
b_u [m]	6,000	3,000	3,000
b_d [m]	6,000	30,000	3,500
H [m]	9	11	7
Modaomen Estuary	**Modaomen Waterway**	**Hongwan Channel**	**Modaomen Channel**
L [km]	150	17	12.5
b_u [m]	2,000	500	2,000
b_d [m]	2,000	3,500[a]	2,000
H [m]	8	5	7

[a]The Hongwan Channel is modeled as a straight channel for the first 11 km, while in the last 6 km of the channel its width increases from 500 to 3,500 m.

where a bar indicates a depth-averaged quantity and a prime the variation from the depth-averaged value. Here, T_Q is the salt transport due to advection by the depth-averaged current, T_E is the salt transport by the exchange flow, and T_D is the salt transport due to horizontal diffusion. Note that the unit of T in Equation 13 is g kg^{-1} m^3 s^{-1}. Hereafter, values of T will be given in kg s^{-1}, which results from multiplication of T with ρ_0/1,000, where ρ_0 = 1,000 kg m^{-3} is the density of fresh water.

From integration of the salt balance over the cross-section, it follows that in each channel T is constant. In particular, $T = 0$ in the river channel, because no salt enters from the river and the lateral boundaries are impermeable. In a network of channels, T is generally nonzero, except in the river channels. Thus, in the geometry displayed in Figure 2a, $T_1 = 0$, but there can be net salt transport from Channel 2 through the junction to Channel 3, or vice versa. This salt transport is the salt overspill T_o. Because $T_1 = 0 = T_2 + T_3$ (from integrating Equation 10d, i.e., conservation of salt at the junction), the overspill in this geometry is given by

$$T_o = -T_2 = T_3. \tag{14}$$

So, by convention T_o is positive when salt is exported from Channel 2 into Channel 3.

2.3. Set-Up of the Simulations

To study the properties of salt overspill, numerical simulations are conducted for model settings that resemble conditions in two estuaries with different characteristics. The first estuarine network concerns the seaward part of the Yangtze Estuary (YE), China, where the South Channel (SC) splits into the South Passage (SP) and the North Passage (NP). The second network is a part of the Pearl River Delta (China), called the Modaomen Estuary (ME), where the Modaomen Waterway (MW) splits into the Hongwan Channel (HC) and the Modaomen Channel (MC). Maps of these deltas are displayed in Figure 1, where it is clear that the geometry of these cases are quite different. The geometrical properties of the channels used in the model are listed in Table 1. The adjacent sea section is for all cases modeled as a 25 km long section with a convergence length of 2.5 km.

3. Results

3.1. Reference Simulations

Before specifically addressing the first objective, reference simulations are conducted where representative values for the dry season are selected for river discharge Q_{riv} and tidal current amplitude U_T. For the Yangtze Estuary, we set Q_{riv} = 4,000 m^3 s^{-1} (J. Wang et al., 2021) and s_{oc} = 25 g/kg (J. Zhu et al., 2018). For each channel, a different value of U_T is used, because this quantity depends strongly on channel geometry (Buschman et al., 2010). The model of J. Wang et al. (2021), which calculates tidal sea surface heights and tidal velocities in a network of estuarine channels, is applied to obtain tidal current amplitudes from imposed tidal sea surface heights at the estuary

mouths, indicated by ζ. We assume ζ to have the same value on all estuary mouths. For the Yangtze, $\zeta = 1.8$ m is imposed for the reference simulation, which gives $U_T = 1.39$, 1.97, and 1.40 m s^{-1} for the South Channel, South Passage, and North Passage, respectively. For the Modaomen Estuary, we set $Q_{riv} = 2{,}000$ m^3 s^{-1}, based on Gong et al. (2012), and $s_{oc} = 35$ g/kg, while $\zeta = 0.875$ m (Gong et al., 2022), resulting in $U_T = 0.84$, 1.05 and 0.75 m s^{-1} for the Modaomen Waterway, Modaomen Channel, and Hongwan Channel respectively.

The tidally mean water level at the ocean (see Equation 9) cannot easily be determined from measurements, but its value has a substantial effect on the net water transport in the channels, because it generates a current from one outlet to another. For the reference simulation, we choose its value so the river discharge distribution agrees with literature, and we keep this value fixed afterward. We find for the YE that $\eta_{oc,SP} - \eta_{oc,NP} = 0.5$ mm, so about 52% of the water from the SC is transported through the NP (Alebregtse & de Swart, 2016; J. Wang et al., 2021) for the reference case. For the ME, we use the observations from L. Zhu et al. (2021), who found that 8.8% and 3.7% of the net water transport is through the HC, for spring and neap tide, respectively, while the river discharge was 2,500 m^3 s^{-1} in the meantime. This gives $\eta_{oc,HC} - \eta_{oc,MC} = 2$ mm. The sensitivity to these values will be discussed in Section 4.

Finally, numerical parameters have to be specified. The horizontal grid size is 50 m in the channels connected to the sea. In the channel connected to the river, grid size increases from 100 m close to the junction to 1,000 m further upstream. In the vertical 10 Fourier modes are used. For both estuaries, a simulation is conducted, where for the equilibrium situation the salt field, overspill, and related quantities are calculated.

Figure 3 shows the steady salt pattern of the reference cases for the YE and the ME. For the YE (panels a and b), the NP is stronger stratified than the SP. Around the junction, salinity is about 1 g/kg. In the NP, a local maximum in bottom salinity is observed around the junction. For the ME (panels c and d), salinity has comparable values around the junction as in the YE, despite the channels being shorter. Both channels are substantially stratified.

The net water transport, depth-averaged salinity distribution, and overspill T_o in the YE are displayed in Figure 4a. The overspill is from the SP into the NP. The salt overspill is 51% of the total seaward salt transport by the depth-averaged current at the junction, making it a major contribution to the salt transport there and thus to salinity in the upstream part of the NP. To determine the underlying mechanisms of the overspill, Figures 4b–4d

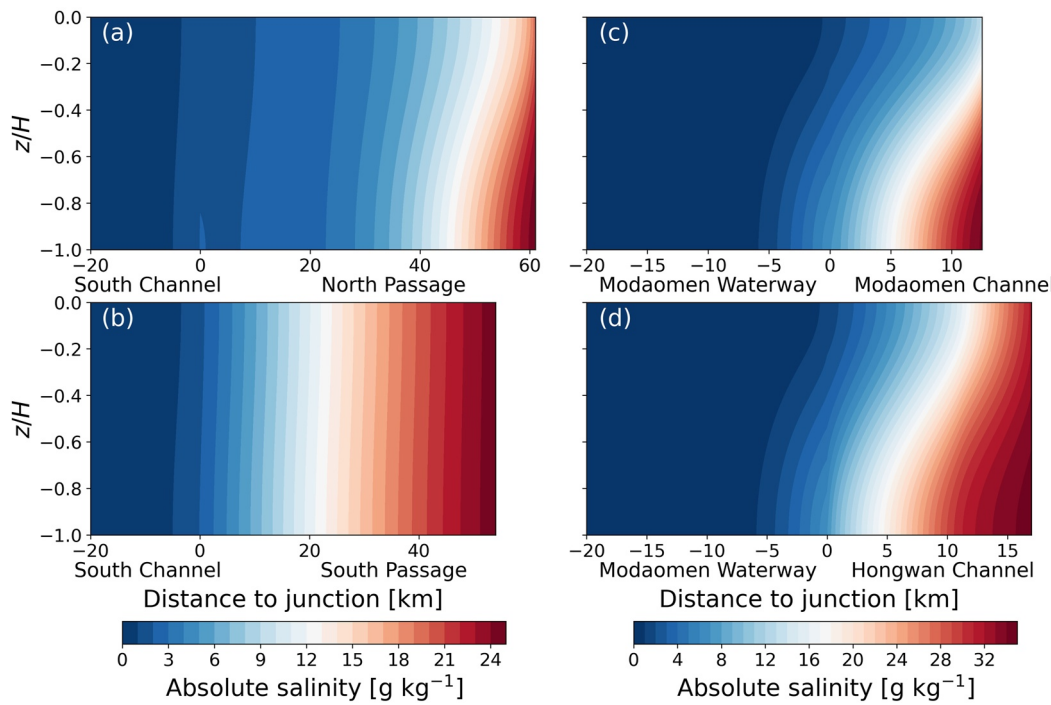

Figure 3. (a) Absolute salinity versus the distance to the junction and $\frac{z}{H}$ in the North Passage (and part of the South Channel) for the reference simulation. (b) As (a), but for the South Passage (and part of the South Channel). (c) As (a), but for the Modaomen Channel (and part of the Modaomen Waterway). (d) As (a), but for the Hongwan Channel (and part of the Modaomen Waterway).

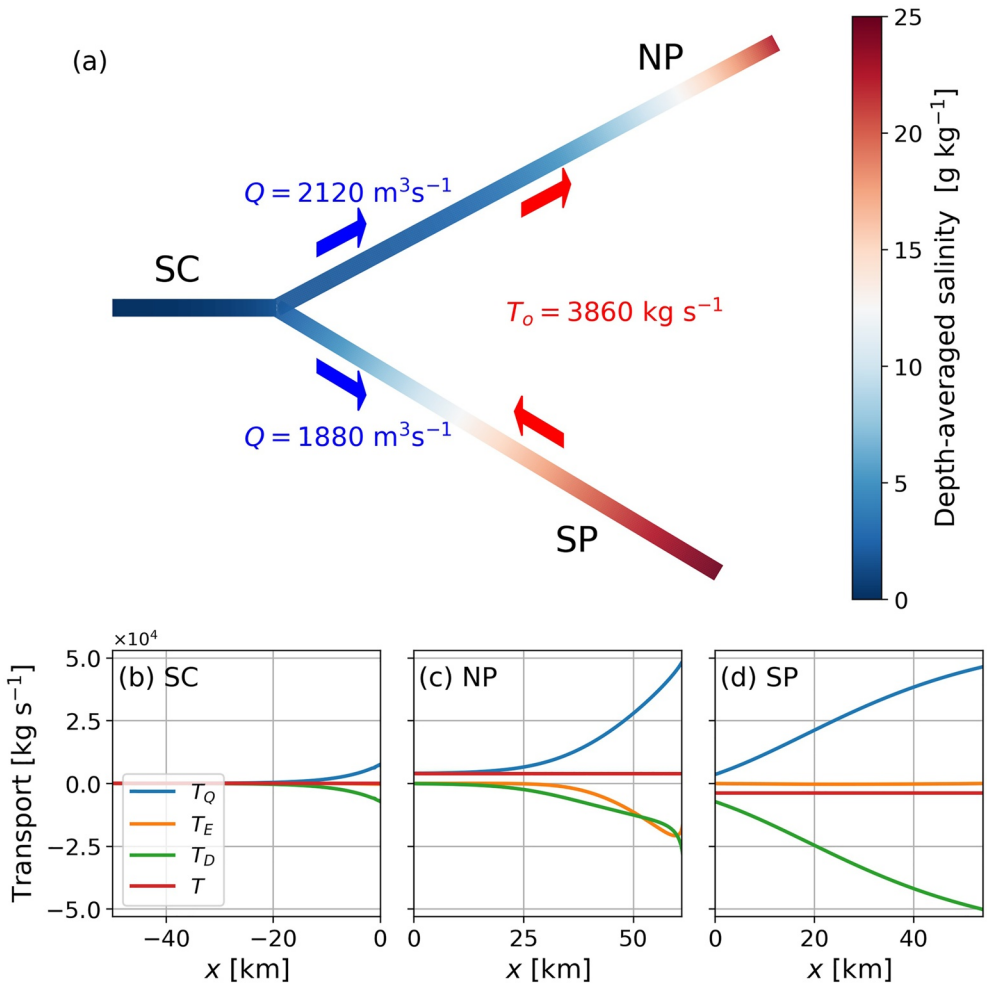

Figure 4. (a) Schematic overview of the depth-averaged salinity, overspill, and river discharge distribution in the Yangtze Estuary for the reference simulation. (b) Salt transport versus x split into the different terms in Equation 13 for the South Channel. (c) As (b), but for the North Passage. (d) As (b), but for the South Passage.

display the spatial patterns of the different components of salt transport (T_Q, T_E, T_D, see Equation 13) in the three channels of the YE. In the SC (panel b), export of salt by the net water transport T_Q (the blue curve) is balanced by import through horizontal diffusion T_D (the green curve), while the contribution of exchange flow T_E (the orange curve) is negligible. In the NP (panel c), the contribution to the import of salt by horizontal diffusion and exchange flow are of comparable magnitude. In the SP (panel d), salt is imported by horizontal diffusion, which exceeds export T_Q in this channel, and is thus the process responsible for the overspill. Horizontal diffusion in this channel is strong, because the converging shape results in strong tidal currents and a weak depth-averaged seaward current.

The discharge distribution and overspill in the ME are visualized in Figure 5a. The discharge in the HC is only 4.9% of the river discharge. The overspill is from the HC into the MC. The magnitude of the overspill is 12% of the total seaward transport by the depth-averaged current at the junction, making it a small contribution to the salinity in the MC. The different components of net salt transport T are displayed in Figures 5b–5e. The salt transport through the HC is much smaller than in the other channels. In all three channels, the contribution of the exchange flow and the horizontal diffusion to salt import are of equal order of magnitude, with the exchange flow being slightly stronger in most of the domain. In the HC, the salt export by the weak depth-averaged current is smaller than the salt import, which causes a net upstream salt transport in this channel, resulting in overspill into the MC.

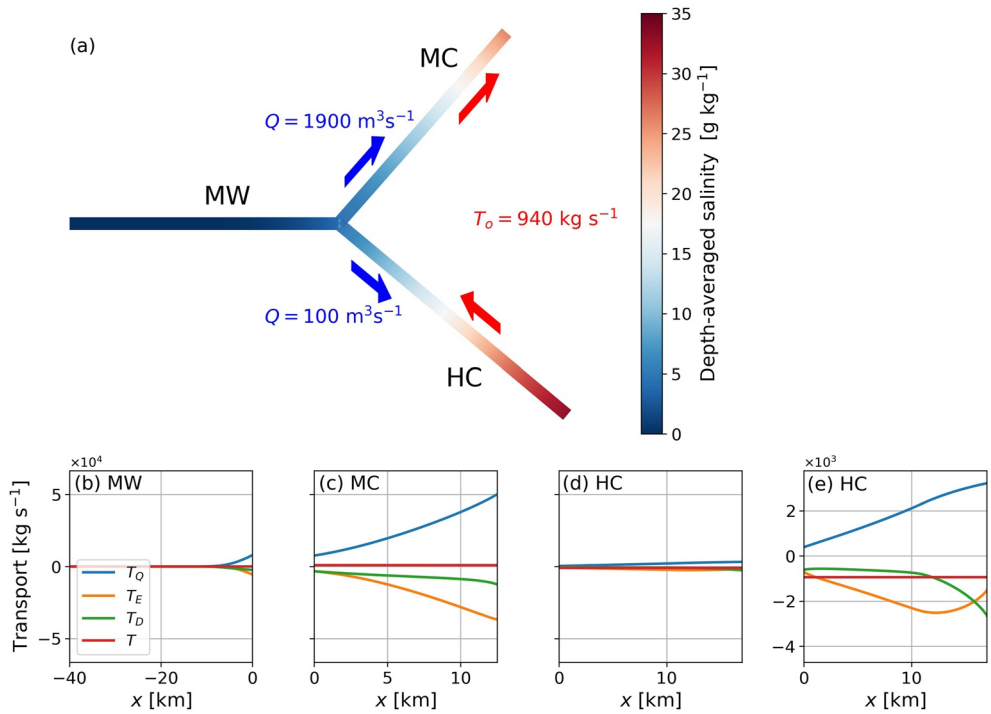

Figure 5. (a) Schematic overview of the depth-averaged salinity, overspill, and river discharge distribution in the Modaomen Estuary for the reference simulation. (b) Salt transport versus x split into the different terms in Equation 13 for the Modaomen Waterway. (c) As (b), but for the Modaomen Channel. (d) As (c), but for the Hongwan Channel. (e) As (d), but with a different y-axis scale.

3.2. An Approximate Expression for Overspill

To explain the properties of overspill from basic physics (the first objective as specified in Section 1), an approximate expression is derived for overspill. The derivation can be found in Appendix A. The expression reads

$$\tilde{T}_o = \begin{cases} -Q_2 s_{oc}, & \text{if } Q_2 < 0, \\ Q_3 s_{oc}, & \text{if } Q_3 < 0, \\ F\ (\tilde{s}_2 - \tilde{s}_3), & \text{otherwise.} \end{cases} \tag{15}$$

In this expression, $\tilde{T}_o$ is the approximate overspill, and $\tilde{s}_2$ and $\tilde{s}_3$ are the values of salinity that the different channels would have at the junction without the conditions for salinity at the junction. Furthermore, $F = \left(\frac{\beta_2}{Q_2} + \frac{\beta_3}{Q_3}\right)^{-1}$ is a factor which mainly quantifies how the discharge is distributed over the channels. It contains known, dimensionless, positive constants β_2, β_3, that depend on the parameters of the system. To compute the parameters on the right-hand side of Equation 15, analytical expressions are given in Appendix A. Equation 15 gives an intuitive understanding of the direction and magnitude of overspill. When the depth-averaged current is from the ocean to the junction, a good estimate of overspill is the strength of this depth-averaged current multiplied with the salinity of the ocean. When this is not the case, the channels can be considered as single channels and the salinity at their upstream limit, that is the junction, can be calculated. The strength and sign of the overspill is linearly related to the difference between these values.

The procedure to use Equation 15 for quantitative approximations of overspill is as follows. When the depth-averaged current in one of the channels is toward the junction, the approximate overspill is directly found from Equation 15. When this is not the case, for both channels separately the salinity at the junction is calculated analytically, assuming no overspill and taking the exchange flow and diffusive limit (Chatwin, 1976). The highest values (either from taking the exchange flow or the diffusive limit) for salinity at the junction are used for $\tilde{s}_2$

and $\tilde{s}_3$, and β_2 and β_3 are calculated afterward. With these parameters, $\tilde{T}_o$ can be calculated. The approximation is valid when $T_2 \ll Q_2 s_{oc}$ and $T_3 \ll Q_3 s_{oc}$, which means that the overspill is relatively small with respect to the total seaward salt transport in both channels. Note that from this procedure we also find whether the depth-averaged current, the exchange flow or horizontal diffusion is the major contributor to salinity at the junction and thus to overspill.

To find if Equation 15 contains the adequate physical behavior, $\tilde{T}_o$ is calculated for the two reference cases. Salinities at the junction without salt transport at the junction are $\tilde{s}_{NP} = 0.0$ g kg^{-1}, $\tilde{s}_{SP} = 3.6$ g kg^{-1}, $\tilde{s}_{MC} = 6.9$ g kg^{-1}, and $\tilde{s}_{HC} = 10.8$ g kg^{-1}, where the subscript indicates the associated channel. This gives $\tilde{T}_o = 3,830$ kg s^{-1} for the YE and $\tilde{T}_o = 1,070$ kg s^{-1} for the ME. The number for the YE is in excellent agreement with the numerical results, and the value for the ME differs by about 15% of the numerical calculated value. Furthermore, the major processes contributing to overspill are, according to the procedure outlined in Appendix A, horizontal diffusion in the NP and SP, and advection due to the exchange flow in the MC and the HC. This is in agreement with what is shown in Figures 4 and 5, justifying the use of Equation 15 to find which salt transport processes are dominant in the seaward channels of the network, provided that the overspill is small compared to the total seaward salt transport in both channels.

3.3. Effect of Tidal Strength and River Discharge on Salt Overspill

To determine the sensitivity to different values of physical parameters, the values of Q_{riv} and ζ are varied (Objective 2 in Section 1), while all other parameters remain the same as the reference simulation. For the Yangtze Estuary, Q_{riv} varies between 1,000 and 10,000 m^3 s^{-1} and for the Modaomen Estuary, Q_{riv} is varied from 400 to 4000 m^3 s^{-1}. Values of the tidal strength are varied from their neap-tide to their spring-tide values, and corresponding values for U_{T} are calculated. For the YE, ζ varies from 1.3 to 2.3 m and for the ME the lowest value of $\zeta = 0.5$ m and the upper value is 1.25 m, based on the maximum and minimum observed range (Gong et al., 2022; Zhang et al., 2016). For each combination of Q_{riv} and U_{T} solutions of the model are determined.

Figure 6 displays salt overspill in the systems as a function of river discharge and tidal strength. For the YE (Figure 6a), we find that there is a maximum in the overspill for moderate values of river discharge. Stronger tides lead to more salt overspill. For the ME (Figure 6b), the largest values of overspill from the HC into the MC occur for low values of river discharge and tidal strength. For stronger river discharge and tides, the overspill changes sign.

We will explain the dependencies found with help of Equation 15. As is shown in Figure S1 in Supporting Information S1, except for some parts of the parameter space in the ME (which will be discussed below), Equation 15 shows the same dependence on the input parameters as the numerical model. For completeness, the strength of

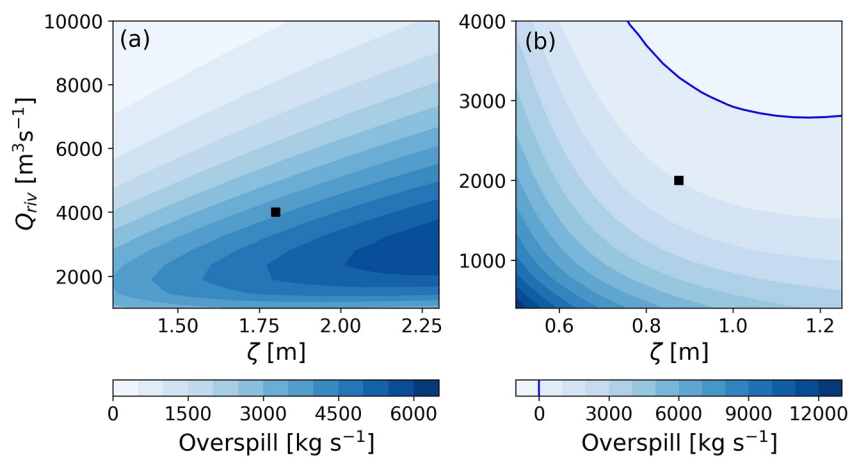

Figure 6. (a) Salt overspill in the Yangtze Estuary versus tidal strength ζ and river discharge Q_{riv}. Positive values indicate overspill from the South Passage into the North Passage. The black square indicates the parameter values of the reference simulation. (b) As (a), but for the Modaomen Estuary. Positive values indicate overspill from the Hongwan Channel into the Modaomen Channel. The blue line indicates where the overspill changes sign.

the tidal currents in both channels and the river discharge distributions are displayed in Figure S2 in Supporting Information S1.

Figure 7a shows which process is the most important for overspill in the channels of the YE for different values of river discharge and tidal strength. This is determined with the method described in Appendix A. It turns out that for almost all considered cases horizontal diffusion is the dominant salt intrusion mechanism in both channels. Panels b and c show the approximations of the salinities at the junction $\tilde{s}_{NP}$ and $\tilde{s}_{SP}$ without salt transfer between the channels (see Equation 15). This indicates that in both channels salinity at the junction decreases with increasing river discharges, and salinity increases with increasing tidal strength, which are well-known characteristics of diffusive estuarine channels. Because $\tilde{s}_{NP}$ (panel b), is less sensitive to changes in forcing than $\tilde{s}_{SP}$ (panel c), the difference between these two quantities increases for stronger tides and lower river discharge. This results in increasing overspill for stronger tides and weaker river discharge. The factor F in Equation 15 is plotted in panel d. This factor increases for larger river discharge, and is thus anti-correlated with $\tilde{s}_{SP} - \tilde{s}_{NP}$. This explains the overspill maximum for river discharge around 3,000 $m^3\ s^{-1}$.

The most important processes contributing to overspill in the ME, calculated with the procedure outlined in Appendix A, are shown in Figure 7e. In the white area, discharge in the HC is negative, that is, mean flow is directed toward the junction. Discharge changes sign, because the pressure gradient due to water level difference between the estuary mouths exceeds the pressure gradient exerted by the river flow in the HC. In this case, all salt transport terms (T_Q, T_E, T_D in Equation 13) are directed toward the junction in the HC and thus strong overspill will occur for low river discharge. When discharge in the HC is toward the ocean, advection by the exchange flow

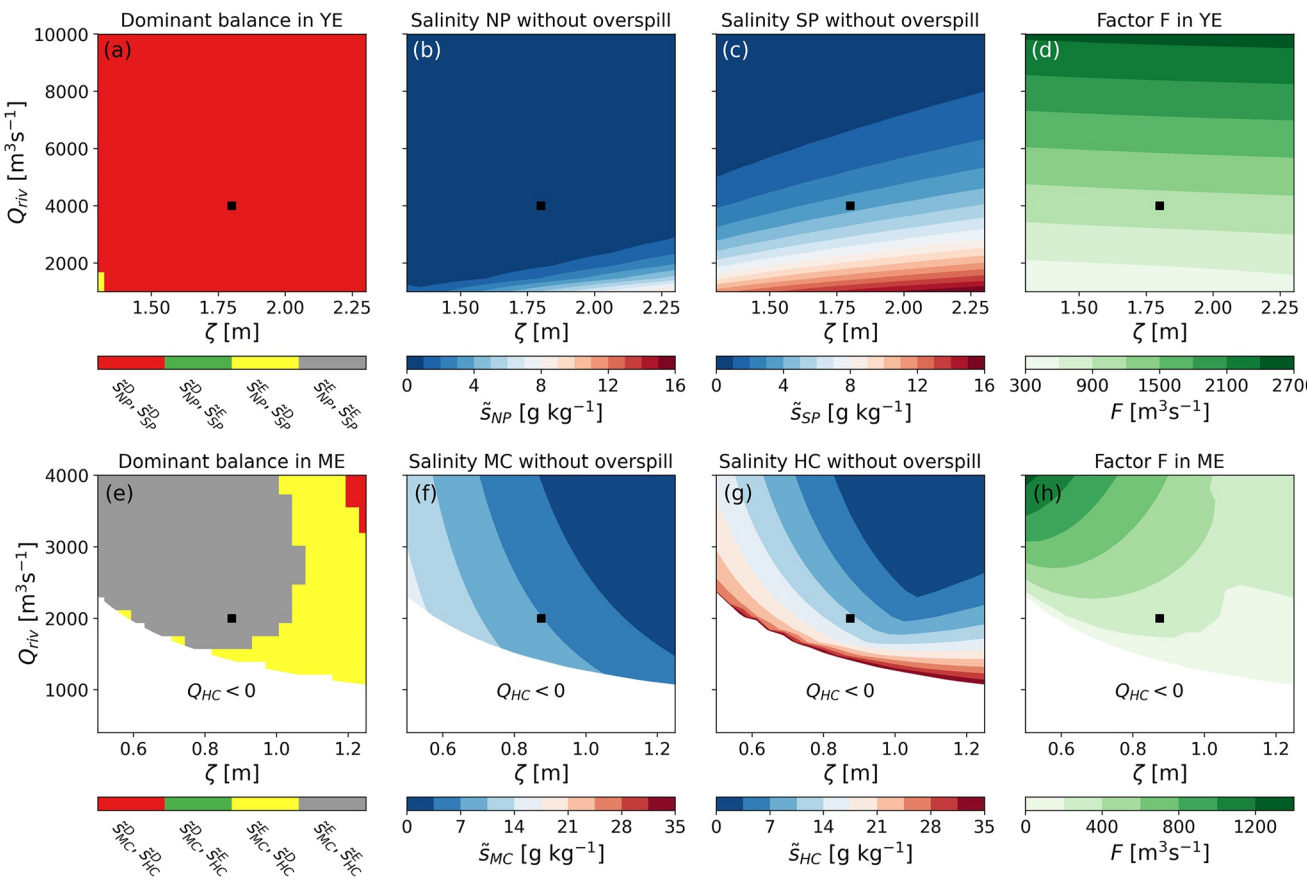

Figure 7. (a) Visualization which balance gives the highest value for salinity at the junction without overspill in both channels, versus tidal strength ζ and river discharge Q_{riv}. Superscript E indicates that the exchange flow limit gives the highest value for $\tilde{s}$ and superscript D indicates that the horizontal diffusion limit gives the highest value. The subscript denotes the specific channel. The black square indicates the parameter values of the reference simulation. (b) As (a), but for the salinity at the junction in the North Passage when there would be no salt transport at the junction. (c) As (b), but for the South Passage. (d) As (a), but for the factor F in Equation 15 for the Yangtze Estuary. (e) As (a), but for the Modaomen and Hongwan Channel of the Modaomen Estuary. (f) As (b), but for the Modoamen Channel. (g) As (b), but for the Hongwan Channel. (h) As (d), but for the Modaomen Estuary. The white area in panels (e)–(h) indicates where $Q_{HC} < 0$.

Table 2
Ranges of Geometrical Properties of the Different Channels Used for the Sensitivity Analysis, Where b_d Is the Width at the Downstream Limit of the Channel (i.e., the Estuary Mouth)

	South Passage	North Passage	Hongwan Channel	Modaomen Channel
b_d [m]	5,000–50,000	2,000–5,000	500–3,500[a]	1,000–3,000
H [m]	7–17	5–12.5	3–10	5–12.5

[a]For the Hongwan Channel the first 11 km is kept as a straight channel of 500 m wide and only the width of the last 6 km is varied.

is dominant in both channels for weak tides, but horizontal diffusion becomes important in the HC for stronger tides. Salinity at the junction without overspill in the MC (panel f) is less sensitive to changes to river discharge or tidal amplitude than the same quantity in the HC (panel g). This means that for weak tides the salinity difference $\tilde{s}_{HC} - \tilde{s}_{MC}$ is large, explaining why there is strong overspill for weak tides. The factor F in Equation 15 reinforces this effect (panel h). However, for high values of river discharge and moderate to strong tides, the salinity difference $\tilde{s}_{HC} - \tilde{s}_{MC}$ decreases and eventually becomes negative, which means that the overspill from the HC into the MC vanishes and changes direction. Note that close to $Q_{HC} = 0$ the conditions under which Equation 15 is valid are not fulfilled, and $\tilde{T}_o$ gives a poor approximation of the overspill T_o. Also, for strong tides, $\tilde{s}_{HC}$ is overestimated, which is because the geometry used in the approximate expression for the HC is slightly different than in the numerical model.

3.4. Effect of Geometry on Salt Overspill

To find the sensitivity of the overspill to changes in geometry (Objective 3 in Section 1), the geometrical properties of the channels in the model are varied. Four series of simulations are done, where in each series the width and depth of one of the channels is varied. Changes to the width are performed by keeping the width at the junction b_u constant and adjusting the downstream width at the estuary mouth b_d, while the width in the rest of the channel is determined with use of Equation 1. Table 2 contains information about the ranges over which these two parameters are varied.

Figure 8 displays the salt overspill when varying the geometry of the channels through the parameters H and b_d. For the North Passage of the YE (Figure 8a), we see that there is a maximum value for overspill for a depth of 13 m, and that increasing the width increases the overspill, but this effect becomes smaller for larger widths. Increasing the width of the SP increases the amount of overspill (Figure 8b), but the sensitivity to the depth of the SP is small. For depths around $H = 9$ m, a maximum exists. Figure 8c shows that increasing the width or the depth of the MC results in more overspill. For a narrow and shallow MC, overspill will change direction. Finally, Figure 8d shows that overspill strongly increases when deepening the HC. However, changes to the width of this channel have little effect.

The response to variations of the geometry can be explained again from Equation 15, since the overspill calculated with this equation contains the same dependency on the geometry as the numerical model, as justified in Figure S3 in Supporting Information S1. For completeness, Figure S4 in Supporting Information S1 shows the tidal currents and river discharge distributions for the different simulations. Regarding the NP, Figure 9a shows

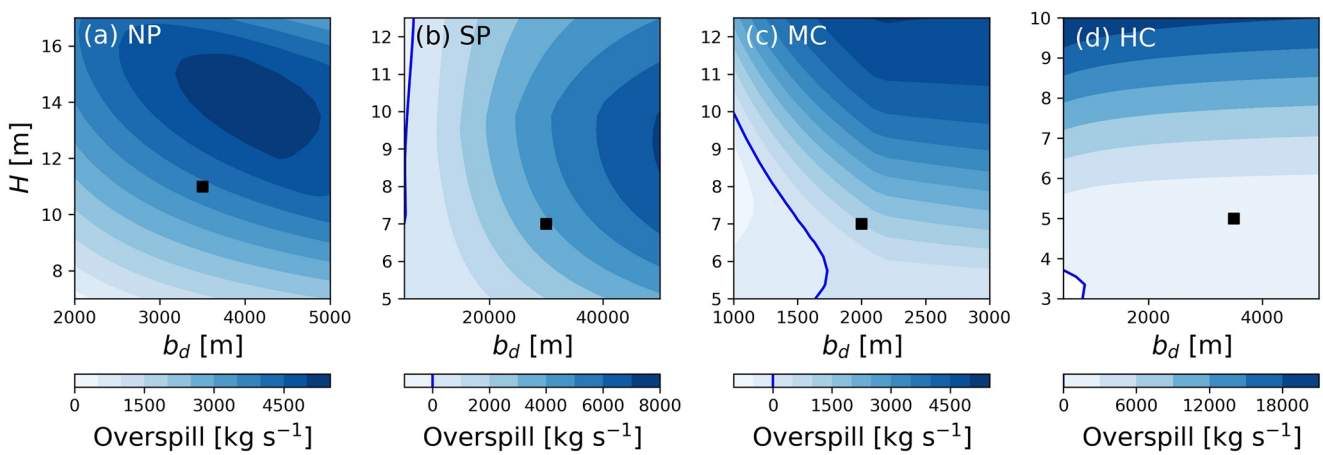

Figure 8. (a) Salt overspill versus width and depth at the mouth of the North Passage. The black square indicates the geometry of the reference simulation. (b) As (a), but for the South Passage. The blue line indicates where overspill changes sign. (c) As (a), but for the Modaomen Channel. (d) As (a), but for the Hongwan Channel.

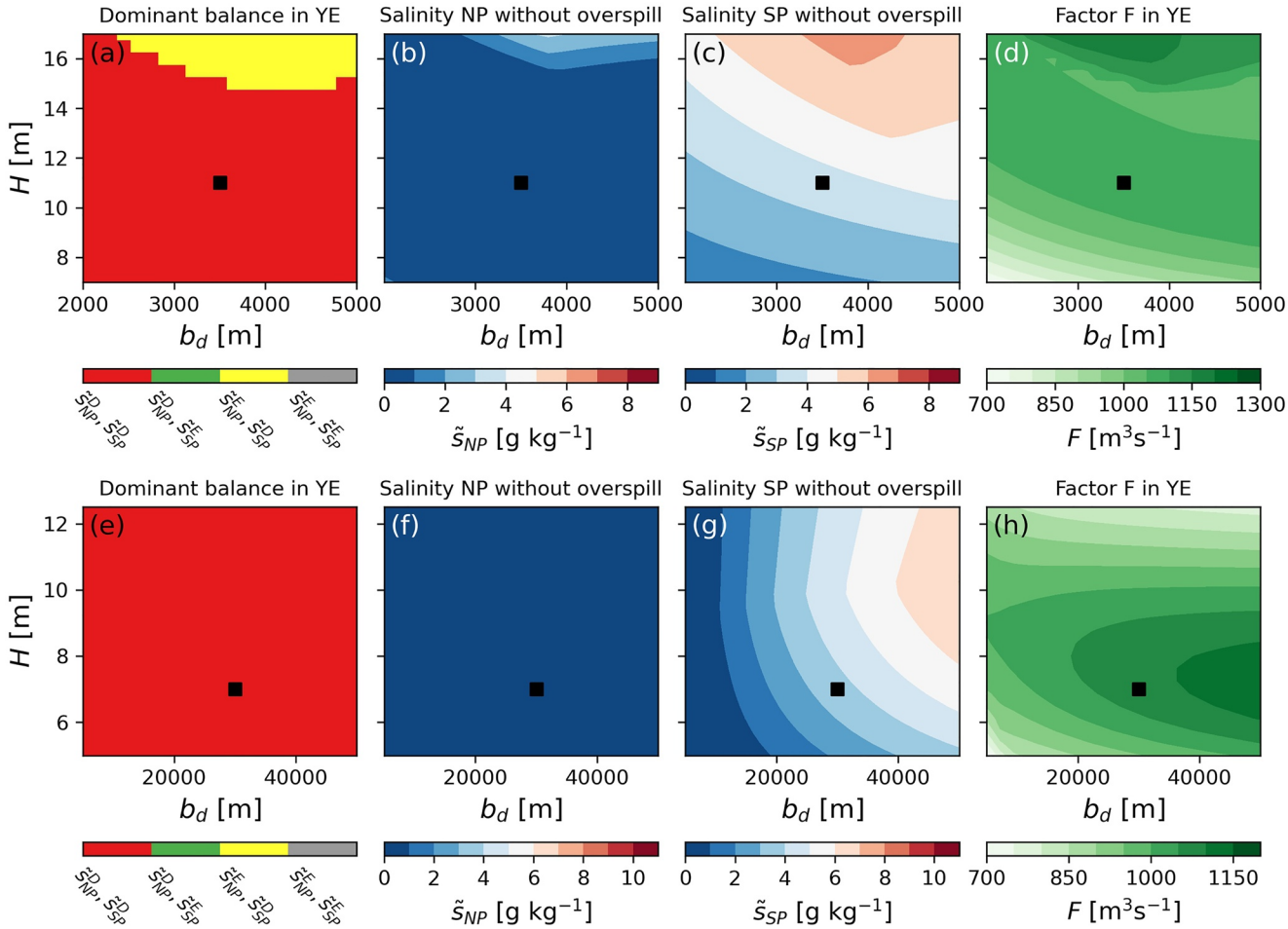

Figure 9. (a) Visualization which balance gives the highest value for salinity at the junction without overspill in both channels, versus width at the estuary mouth b_d and depth H of the North Passage. Superscript E indicates that the exchange flow limit gives the highest value for $\tilde{s}$ and superscript D indicates that the horizontal diffusion limit gives the highest value. The subscript indicates the concerning channel. The black square indicates the parameter values of the reference simulation. (b) As (a), but for salinity at the junction in the North Passage when there would be no salt transport through the junction. (c) As (b), but for the South Passage. (d) As (a), but for the factor F in Equation 15. (e) As (a), but versus width at the estuary mouth and depth of the South Passage. (f) As (e), but for salinity at the junction in the North Passage when there would be no salt transport through the junction. (g) As (f), but for the South Passage. (h) As (e), but for the factor F in Equation 15.

that, except for large depths, horizontal diffusion is the dominant salt import process in both channels. Increasing the width or depth of the NP will cause more water to flow through the NP and suppress salt intrusion in this channel. However, as salt intrusion in this channel does not reach the junction (Figure 9b), this suppression of salt intrusion in the NP has no effect on the overspill. On the other hand, the SP will receive less water from the SC, increasing the amount of salt reaching the junction from this channel (Figure 9c), thus increasing the amount of overspill for a deeper or wider NP. Figure 9a shows that for large depths advection by the exchange flow becomes more important than horizontal diffusion in the NP. This allows salt from the NP to reach the junction (upper part of Figure 9b), decreasing the strength of overspill for large depths. This results in the maximum for overspill for depths around 13 m, which is the maximum depth for which salinity from the NP still does not reach the junction. Figure 9d shows that the factor F in Equation 15 does not vary strongly when changing the geometry of the NP.

For the SP, we find that horizontal diffusion has the largest contribution to salt import in both channels for all geometries (Figure 9e). There is no salt through the NP reaching the junction (Figure 9f), so the amount of overspill is solely determined by the amount of salt reaching the junction through the SP, displayed in Figure 9g. This amount increases for a wider SP, because the depth-averaged current in a single channel is inversely proportional to the width, while the share of the discharge the channel receives at the junction is weaker than proportionally related to the width (see Equation 12). This indicates that the seaward salt transport due to the depth-averaged current T_Q decreases for a wider channel. In addition, the salt import by horizontal diffusion T_D will increase

because the tidal current increases for a wider SP. These effects intensify each other and the overspill increases for a wider SP. Regarding depth, there is an overspill maximum observed for depths of about 9 m. This maximum is a result of the combined effects of the depth on tidal current and river discharge. Deepening the SP leads to an increase in tidal current and thus in horizontal diffusion, which leads to increasing overspill for small depths. For larger depths, the effect on the discharge distribution dominates: a deeper SP will receive more discharge, which is stronger than the effect of the weakening of the depth-averaged current, and decreases the salt overspill through this channel. This effect is visible in the factor F (Figure 9h).

Figure 10a shows that the dominant processes importing salt in the ME depend strongly on the geometry of the MC. For most values of the parameters, the depth-averaged current in the HC is toward the junction. The deeper and wider the MC is, the stronger this current will be (see Equation 12), and this is associated with an increase in overspill. For a narrow MC, the tidal current will increase in the MC, with the consequence that horizontal diffusion becomes more important. Hence, the amount of salt at the junction originating from the MC will be of equal magnitude as the amount from the HC (Figures 10b and 10c). This causes the overspill to decrease with decreasing width and eventually to change its sign. The difference $\tilde{s}_{MC} - \tilde{s}_{HC}$ is small for this situation, compared to differences in other parts of the parameter space, but the factor F in Equation 15 is large (Figure 10d). Because of this, the overspill to the HC is not negligible here.

For a shallow HC, Figure 10e shows that horizontal diffusion is the dominant salt import process in this channel, because the tidal velocity is large for this geometry. For a deeper HC, advection by the exchange flow is the dominant process. In the MC, exchange flow is the dominant process, irrespective of the geometry of the HC. This

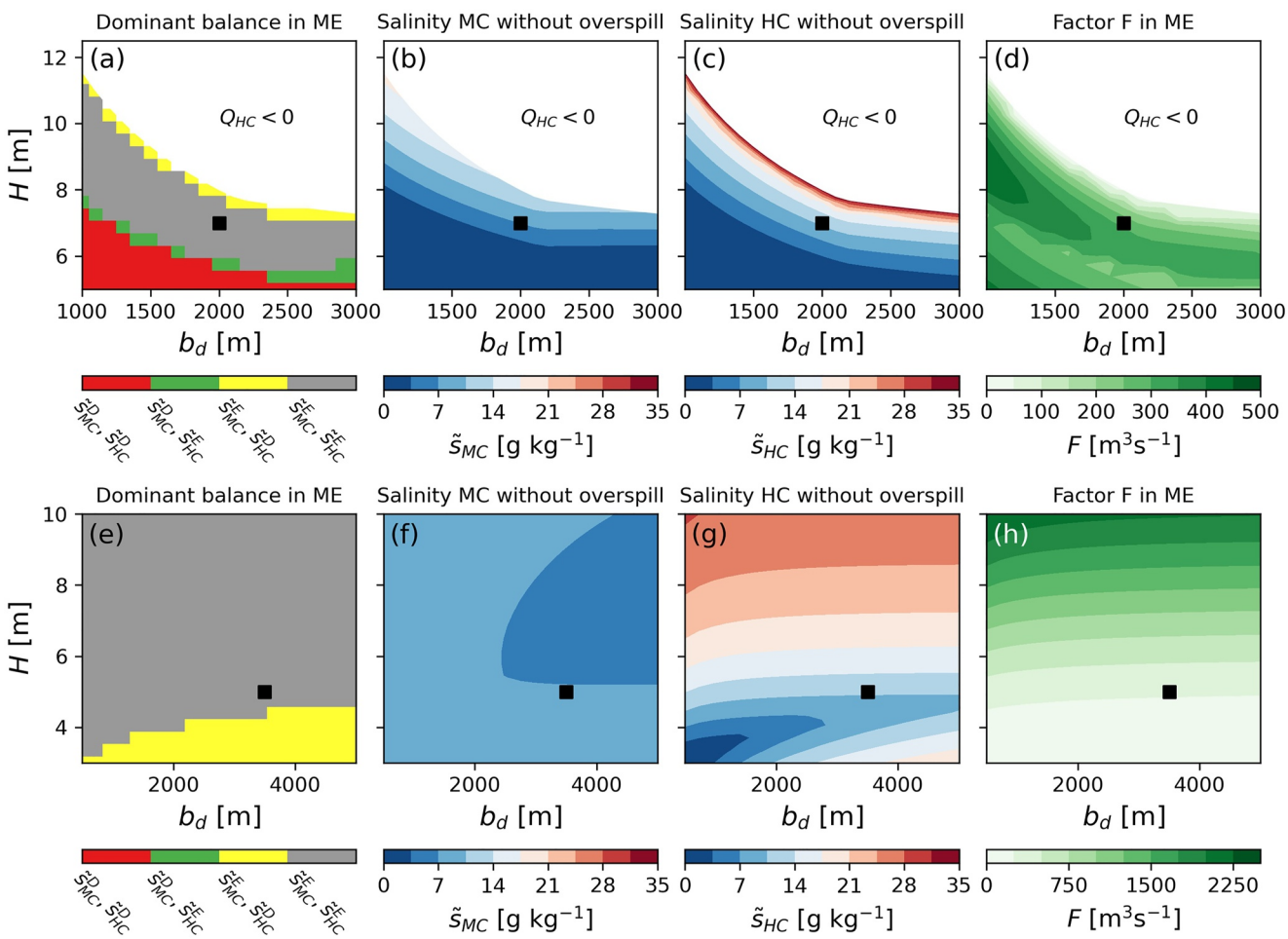

Figure 10. As Figure 9, but for variations of the width at the estuary mouth b_d and depth H of the Modaomen Channel ((a)–(d)) and to the Hongwan Channel ((e)–(h)) of the Modaomen Estuary. The white area in panels (a)–(d) indicates where $Q_{HC} < 0$.

results in an almost constant amount of salt reaching the junction through the MC (Figure 10f), independent of the geometry of the HC. In the HC two maxima are visible for $\tilde{s}_{HC}$ (Figure 10g): one for small depths and large widths when horizontal diffusion dominates, and another for large depths when the exchange flow is the dominant process importing salt. However, Figure 10h shows that F is very small for a shallow HC, because the discharge in the different channels differs strongly. This means that there is only little overspill in this regime (see Equation 15). For larger depths, the salinity from the HC increases with depth, because the strength of the exchange flow increases for a deeper channel. In addition, F increases, because the discharge is more equal between the channels. These effects reinforce each other, resulting in large values of overspill. The weak dependence on width compared to that on depth is mostly due to the fact that the changes to the volume of the HC by changes in width are much smaller than to changes in depth.

4. Discussion

We have used an idealized model to study overspill in a simple estuarine network for different physical forcing parameters and geometries, where the Yangtze and Modaomen Estuary are taken as prototype systems. The quantification and understanding of the sensitivity of the overspill to different physical forcings and geometries is the main new contribution of this study. Our results for the YE agree favorably with those in the literature. The direction of salt overspill that our model computes is in line with what is found by J. Zhu et al. (2018). This study also indicates that tidal pumping is the dominant salt import mechanism of the YE, and thus salt intrusion increases with stronger tides. This is correctly reproduced in our model. Stratification in our idealized representation of the YE also agrees qualitatively with results presented in Hu and Ding (2009), Wu et al. (2010), and Qiu and Zhu (2015). From these results, the effect of anthropogenic modifications on overspill can be estimated. A major modification was the Deep Waterway Project, in which the North Passage was narrowed and deepened from 7 m to an average depth of 11 m (Hu & Ding, 2009; J. Zhu et al., 2006). According to our model results, the deepening has lead to an increase in overspill, while the narrowing lead to a decrease. A further increase in depth would first lead to an increase of overspill. When the depth would exceed 13 m, salt intrusion through the NP will reach the junction, which leads to a decrease in the overspill but to a strong increase in salinity in the NP.

Regarding the ME, Gong and Shen (2011) and Gong et al. (2012) indicate that this estuary is partially mixed during the dry season, which is in line with our model results. Gong et al. (2012) also mention that the most important mechanism for salt import is the exchange flow, and thus the salt intrusion and overspill increase for a weaker tidal current. This is reproduced by our model. For the geometry, Liu et al. (2019) demonstrated that changing the depth of the Modaomen Channel has a larger effect on salt intrusion than changing the width, in agreement with what we demonstrated and explained. Gong et al. (2014) noticed that the overspill is time dependent in the ME, but did not specify the forcing-overspill relationship from the available observations. Our sensitivity analysis indicates that overspill is susceptible to changing direction when varying the tidal forcing over the observed range in the spring-neap cycle, or varying the river discharge over realistic values for the dry season. We demonstrated that overspill is from the HC into the MC for low values of river discharge or tidal strength, but for higher values of these quantities the overspill reverses direction. The modeling studies, of Gong et al. (2012) (their Figure 12) and B. Wang et al. (2012) (their Figure 8) found that, using a high-resolution numerical model, the main mechanism of salt overspill is salt transport by net water transport from the ocean to the junction through the HC. In our results, this is the case for low values of river discharge. We additionally showed that without the depth-averaged current being toward the junction, exchange flow is capable of driving overspill from the HC into the MC. Finally, in Gong et al. (2014) it is mentioned that "plans have been proposed to set up a sluice at the junction between the Hongwan and Modaomen Waterways for preventing the salt transport from the Hongwan Waterway at flood tides." According to our results, this would be successful in avoiding salt intrusion during the neap tide and periods of low river discharge. However, when the Hongwan Channel would be deepened, overspill from this channel would strongly increase and the proposed sluice would be more effective in preventing extra salinization of the Modaomen Channel.

Our idealized model presented in Section 2 has limitations in modeling of overspill. Intratidal processes are not explicitly captured by the subtidal model. However, the tidal phase difference at the junction between different channels can be important in causing a subtidal transport of salt (Corlett & Geyer, 2020). The width-averaging makes that the currents and salinity in the model do not have a lateral structure, but this can be important for overspill in wide channels, as is shown for example, in Wu et al. (2006) and Xue et al. (2009). The assumption

of steady state also is a limiting factor of this research, as usually the adjustment time of an estuary is larger than the timescale on which the forcing varies, which means that steady state is not attained, as shown for example, in the Modaomen Estuary (Gong & Shen, 2011). Horizontal diffusion of salt turns out to be the dominant process in several scenarios considered. To a large extent, horizontal diffusion mimics unresolved processes, such as horizontal shear dispersion and tidal pumping, which are not explicitly computed because we use width- and tidally-averaged equations. Specifically, horizontal shear dispersion is a complex process that strongly depends on channel properties, such as channel-to-shoal differences in depth, channel width, and curvature (Geyer & Signell, 1992; Huijts et al., 2009; Lerczak et al., 2006; Zimmerman, 1986). Changes in the bathymetry would alter these processes and thereby horizontal diffusivity (Ralston & Geyer, 2019; J. Zhu et al., 2015). Such changes are not explicitly captured by our parametrization of the horizontal diffusion coefficient.

In our model formulation the discharge in the different channels is very sensitive to the water level at the estuary mouths: changes of millimeters have large effects on the discharge. Also, we assumed that water setup due to baroclinic pressure is balanced by a barotropic pressure gradient due to a water level difference between the estuary mouths. Figure S5 in Supporting Information S1 shows that very unrealistic discharges in the channels are obtained when this condition is not satisfied. These model characteristics are due to the fact that the subtidal water level gradient $\frac{\partial \eta}{\partial x}$ is very small (order of 10^{-7}) with our choice of A_v, compared to typical water level gradients due to tides. When A_v would be larger, the relative contribution of the salinity and the water levels at the mouths to the net water transport becomes smaller. However, our formulation of A_v is in line with existing literature (e.g., MacCready, 2004; Ralston et al., 2008). A larger A_v would result in smaller exchange flow and stratification, and thereby in weaker salt intrusion. Our approach is to use a small A_v and assume the contribution of salinity to the water level to be balanced by a barotropic pressure gradient. This is in line with two-dimensional (2D) model studies, which demonstrated that realistic water distributions are obtained without considering salinity (Buschman et al., 2010; J. Wang et al., 2021). Furthermore, 3D models (Maicu et al., 2018) that include salinity showed that the discharge distribution over the channels is only weakly dependent on river discharge, which is not the case in our model if one would include the contribution of salinity to the water distribution. We thus consider these findings as a justification of our assumption.

5. Conclusions

This study aimed at gaining fundamental knowledge of salt overspill at channel junctions and to better understand salt intrusion in an estuarine network. We found from the basic physics that salt overspill in an estuarine network is in the direction of the depth-averaged current, if in one of the channels the depth-averaged current is from the ocean to the junction. The magnitude of overspill is then linearly related to the strength of the depth-averaged current. If the depth-averaged current is toward the ocean in both channels, the sign of the difference in salinity at the junction, when the channels are treated as single channels, determines the direction of overspill. The magnitude of the overspill scales linearly with this difference in salinity at the junction, and with a factor which mainly quantifies how equal the discharge is distributed over the two channels.

A larger river discharge results in weaker salt intrusion and thus less overspill, unless the discharge distribution is very sensitive to changes to the river discharge. Stronger tides lead to more salt intrusion in a tidal horizontal diffusion dominated channel, but to weaker salt intrusion in an exchange flow dominated channel. The resulting effect on the difference in salinity at the junction, when the channels are treated as single channels, determines the response to changes to tidal forcing.

Regarding dependence on the geometry, we found that a wider and deeper channel leads to a larger portion of the discharge that the channel receives, to a weakening of the depth-averaged current and to changes to the tidal currents in the channels. A deeper channel also leads to an increase of vertical viscosity and diffusivity, and to an increase of the exchange flow. The net effect on overspill can be quantified again from the aforementioned procedure. These findings make it possible to quantify and understand the sensitivity of salt transport between channels in estuarine deltas to changes to the river discharge, tidal strength, and width and depth of the channels.

Appendix A: Derivation of an Approximate Expression for Salt Overspill

An approximate expression for overspill $\tilde{T}_o$ in the three-channel network (see Figure 2 in the main text) is obtained as follows. Starting point is the depth integrated salt balance Equation 13, which for convenience is written as

$$\bar{\Sigma} + \frac{bH}{Q}\overline{u'\Sigma'} - \frac{bHK_h}{Q}\frac{d\bar{\Sigma}}{dx} = \hat{T}_o, \qquad \bar{\Sigma}(x=0) = \bar{\Sigma}_0. \tag{A1}$$

In this equation,

$$\bar{\Sigma} = \frac{\bar{s}}{s_{oc}}, \quad \Sigma' = \frac{s'}{s_{oc}}, \quad \hat{T}_o = \frac{T_o}{Qs_{oc}}, \tag{A2}$$

where $\hat{T}_o$ is the dimensionless overspill and $\bar{\Sigma}_0$ is the dimensionless salinity at the ocean boundary. The other variables and parameters have the same meaning as those in the main text.

Together with an equation for Σ', the salinity field can be in principle (at least numerically) determined in any channel for any value of $\hat{T}_o$ and $\bar{\Sigma}_0$, given that the river discharge is known. The overspill (from Channel 2 and Channel 3 or vice versa) subsequently follows by demanding

$$\bar{\Sigma}_2\big|_{\text{jun}} = \bar{\Sigma}_3\big|_{\text{jun}}. \tag{A3}$$

This condition represents continuity of depth-averaged salinity at the junction (indicated by subscript "jun"). Note that the junction is the landward boundary of both Channel 2 and Channel 3.

An approximate expression for overspill can be found when considering different balances in Equation A1.

A1. Diffusive Limit

When $T_D \gg T_E$ in Equation 13, the second term on the left-hand side of Equation A1 can be neglected with respect to the other terms. The solution of the reduced equation, using Equation 1 of the main text for width b, reads

$$\bar{\Sigma} = \hat{T}_o + \left(\bar{\Sigma}_0 - \hat{T}_o\right)\exp\left(\frac{L_b}{L_D}\left[e^{L/L_b} - e^{\frac{x+L}{L_b}}\right]\right). \tag{A4}$$

Here, $L_D = \frac{K_h b_u H}{Q}$ is a diffusive length scale, which depends on Q. From this, it follows that

$$\Sigma\Big|_{\text{jun}} = \hat{T}_o + \left(\bar{\Sigma}_0 - \hat{T}_o\right)\exp\left(\frac{L_b}{L_D}\left[e^{L/L_b} - 1\right]\right). \tag{A5}$$

For the value $\bar{\Sigma}_0$ at the mouth, we use for simplicity a constant value of 1. Note that in principle a better approximation of this quantity could be obtained by using the procedure prescribed in MacCready (2004), but to keep the analysis simple we do not use this here. Substitution of this result in the previous equation yields

$$\begin{aligned} \Sigma\big|_{\text{jun}} &= \mu + (1-\mu)\hat{T}_o, \\ \mu &= \exp\left(-\frac{L_b}{L_D}\left[e^{L/L_b} - 1\right]\right) \quad . \end{aligned} \tag{A6}$$

A2. Exchange Limit

In this case, first considered by Chatwin (1976) for a single channel, the diffusive term in Equation A1 is ignored and the salt flux $\overline{u'\Sigma'}$ is fully determined by the exchange flow. The reduced equation reads

$$\bar{\Sigma} - {L_e}^3\left(\frac{d\bar{\Sigma}}{dx}\right)^3 = \hat{T}_o \quad \text{with} \quad L_e = \left(\frac{48^2}{0.112}\frac{Q}{b(x)H}\frac{A_v^2 K_v}{g^2\beta^2 s_{oc}^2 H^8}\right)^{\frac{1}{3}}. \tag{A7}$$

Note that L_e depends on x (because of width variation) and on Q. The solution of Equation A7 is

$$\Sigma = \hat{T}_o + \left\{\left(\bar{\Sigma}_0 - \hat{T}_o\right)^{2/3} + 2\frac{L_b}{L_e}e^{\frac{-L}{3L_b}}\left[1 - e^{\frac{-x}{3L_b}}\right]\right\}^{3/2}, \tag{A8}$$

in which we choose again $\bar{\Sigma}_0 = 1$. Evaluation of Equation A8 at the landward boundary yields

$$\bar{\Sigma}\Big|_{\text{jun}} = \hat{T}_o + \left\{\left[\left(1-\hat{T}_o\right)\right]^{2/3} - \gamma\right\}^{3/2},$$
$$\gamma = 2\frac{L_b}{L_e}\left[\exp\left(-\frac{1}{3}L/L_b\right) - 1\right]. \tag{A9}$$

For latter use, it is convenient to give the approximate expression for $\bar{\Sigma}\big|_{\text{jun}}$ for $\hat{T}_o \ll 1$. Application of a Taylor expansion yields

$$\bar{\Sigma}\Big|_{\text{jun}} = (1-\gamma)^{3/2} + \left[1-(1-\gamma)^{1/2}\right]\hat{T}_o + \mathcal{O}\left(\hat{T}_o^2\right). \tag{A10}$$

A3. Definition of the Approximate Overspill

To determine which formulation should be used, first it is determined whether there is a negative discharge in one of the channels. If this is not the case, Equations A6 and A9 are evaluated for $\hat{T}_o = 0$. When Equation A6 gives the highest value, horizontal diffusion is the major contributor to salinity at the junction, but when Equation A9 gives the highest value, advection by exchange flow is found to be dominant.

Thus, either of the four following situations will occur: (a) The depth-averaged current in one of the channels is toward the junction; (b) Horizontal diffusion is the dominant process in both Channel 2 and Channel 3; (c) In one channel horizontal diffusion dominates and in the other one advection by exchange flow; and (d) Advection by exchange flow is dominant in both Channel 2 and Channel 3.

Situation 1: Salt import in Channel 2 or Channel 3 is dominated by a depth-averaged current toward the junction

In this case, a first order estimate of the dimensionless salt transport is $\hat{T}_o = 1$. In dimensional coordinates we find

$$\tilde{T}_o = \begin{cases} Q_2 s_{oc}, & \text{if } Q_2 < 0, \\ -Q_3 s_{oc}, & \text{if } Q_3 < 0. \end{cases} \tag{A11}$$

Situation 2: Salt import in Channel 2 and Channel 3 is dominated by diffusion

Substitution of Equation A6 into Equation A3, a linear algebraic equation for $\tilde{T}_o$ is obtained, with solution

$$\tilde{T}_o = s_{oc}\left[\frac{1-\mu_2}{Q_2} + \frac{1-\mu_3}{Q_3}\right]^{-1}(\mu_3 - \mu_2). \tag{A12}$$

Here, μ_2, μ_3 follow from Equation A6 by using the parameters of Channel 2 and Channel 3, respectively.

Situation 3: Salt import in Channel 2 is by diffusion and Channel 3 by exchange flow

This involves the substitution of Equation A6 for Channel 2 and Equation A9 into Equation A3. This results in a nonlinear algebraic equation for $\hat{T}_o$, for which no closed-form solutions exist. Replacing Equation A9 by its first-order Taylor expansion in $\hat{T}_o$, that is, Equation A10, overspill $\tilde{T}_o$ is the solution of a linear algebraic equation:

$$\tilde{T}_o = s_{oc}\left[\frac{1-(1-\gamma_2)^{\frac{1}{2}}}{Q_2} + \frac{1-\mu_3}{Q_3}\right]^{-1}\left(\mu_3 - (1-\gamma_2)^{\frac{3}{2}}\right). \tag{A13}$$

Situation 4: Salt import in Channel 2 and Channel 3 is exchange-dominated

In this case, Equation A10 is substituted into Equation A3, resulting again in a linear algebraic equation for $\tilde{T}_o$. Its solution reads

$$\tilde{T}_o = s_{oc}\left[\frac{1-(1-\gamma_2)^{\frac{1}{2}}}{Q_2} + \frac{1-(1-\gamma_3)^{\frac{1}{2}}}{Q_3}\right]^{-1}\left((1-\gamma_3)^{\frac{3}{2}} - (1-\gamma_2)^{\frac{3}{2}}\right). \tag{A14}$$

Summary

We have to consider four cases, for which a different expression for the overspill is obtained. Taking all these cases together, we find Equation 15 of the main text.

Data Availability Statement

Software used to generate the data and create the figures used in this study is made available online (Biemond, 2023).

Acknowledgments
This work is part of the Perspectief Program SaltiSolutions, which is financed by NWO Domain Applied and Engineering Sciences (2022/TTW/01344701 P18-32 project5) in collaboration with private and public partners.

References

Alebregtse, N. C., & de Swart, H. E. (2016). Effect of river discharge and geometry on tides and net water transport in an estuarine network, an idealized model applied to the Yangtze Estuary. *Continental Shelf Research*, *123*, 29–49. https://doi.org/10.1016/j.csr.2016.03.028

Biemond, B. (2023). Software publication 'Mechanisms of salt overspill at estuarine network junctions explained with an idealized model'. [Software]. Zenodo. https://doi.org/10.5281/zenodo.7673946

Biemond, B., de Swart, H. E., Dijkstra, H. A., & Díez-Minguito, M. (2022). Estuarine salinity response to freshwater pulses. *Journal of Geophysical Research: Oceans*, *127*(11), e2022JC018669. https://doi.org/10.1029/2022JC018669

Buschman, F. A., Hoitink, A. J. F., van der Vegt, M., & Hoekstra, P. (2010). Subtidal flow division at a shallow tidal junction. *Water Resources Research*, *46*(12). https://doi.org/10.1029/2010WR009266

Chatwin, P. (1976). Some remarks on the maintenance of the salinity distribution in estuaries. *Estuarine and Coastal Marine Science*, *4*(5), 555–566. https://doi.org/10.1016/0302-3524(76)90030-X

Corlett, W. B., & Geyer, W. R. (2020). Frontogenesis at estuarine junctions. *Estuaries and Coasts*, *43*(4), 722–738. https://doi.org/10.1007/s12237-020-00697-1

Dijkstra, Y. M., & Schuttelaars, H. M. (2021). A unifying approach to subtidal salt intrusion modeling in tidal estuaries. *Journal of Physical Oceanography*, *51*(1), 147–167. https://doi.org/10.1175/JPO-D-20-0006.1

Eslami, S., Hoekstra, P., Minderhoud, P. S. J., Trung, N. N., Hoch, J. M., Sutanudjaja, E. H., et al. (2021). Projections of salt intrusion in a mega-delta under climatic and anthropogenic stressors. *Communications Earth & Environment*, *2*(1), 142. https://doi.org/10.1038/s43247-021-00208-5

Gao, B., Yang, D., & Yang, H. (2013). Impact of the Three Gorges Dam on flow regime in the middle and lower Yangtze River. *Quaternary International*, *304*, 43–50. https://doi.org/10.1016/j.quaint.2012.11.023

Geyer, W. R., & MacCready, P. (2014). The estuarine circulation. *Annual Review of Fluid Mechanics*, *46*(1), 175–197. https://doi.org/10.1146/annurev-fluid-010313-141302

Geyer, W. R., & Signell, R. P. (1992). A reassessment of the role of tidal dispersion in estuaries and bays. *Estuaries*, *15*(2), 97–108. https://doi.org/10.2307/1352684

Gong, W., Maa, J. P.-Y., Hong, B., & Shen, J. (2014). Salt transport during a dry season in the Modaomen estuary, Pearl River Delta, China. *Ocean & Coastal Management*, *100*, 139–150. https://doi.org/10.1016/j.ocecoaman.2014.03.024

Gong, W., & Shen, J. (2011). The response of salt intrusion to changes in river discharge and tidal mixing during the dry season in the Modaomen Estuary, China. *Continental Shelf Research*, *31*(7–8), 769–788. https://doi.org/10.1016/j.csr.2011.01.011

Gong, W., Wang, Y., & Jia, J. (2012). The effect of interacting downstream branches on saltwater intrusion in the Modaomen Estuary, China. *Journal of Asian Earth Sciences*, *45*, 223–238. https://doi.org/10.1016/j.jseaes.2011.11.001

Gong, W., Zhang, G., Zhang, H., Yu, X., Zhu, L., & Li, S. (2022). The effects of mouth bar on salt intrusion in a partially mixed estuary. *Journal of Hydrology*, *612*, 128261. https://doi.org/10.1016/j.jhydrol.2022.128261

Hansen, D. V., & Rattray, M. (1966). New dimensions in estuary classification 1. *Limnology & Oceanography*, *11*(3), 319–326. https://doi.org/10.4319/lo.1966.11.3.0319

Hu, K., & Ding, P. (2009). The effect of deep waterway constructions on hydrodynamics and salinities in Yangtze Estuary, China. *Journal of Coastal Research*, 961–965.

Huijts, K., Schuttelaars, H., de Swart, H., & Friedrichs, C. (2009). Analytical study of the transverse distribution of along-channel and transverse residual flows in tidal estuaries. *Continental Shelf Research*, *29*(1), 89–100. https://doi.org/10.1016/j.csr.2007.09.007

Lerczak, J. A., Geyer, W. R., & Chant, R. J. (2006). Mechanisms driving the time-dependent salt flux in a partially stratified estuary. *Journal of Physical Oceanography*, *36*(12), 2296–2311. https://doi.org/10.1175/JPO2959.1

Liu, C., Yu, M., Jia, L., Cai, H., & Chen, X. (2019). Impacts of physical alterations on salt transport during the dry season in the Modaomen Estuary, Pearl River Delta, China. *Estuarine, Coastal and Shelf Science*, *227*, 106345. https://doi.org/10.1016/j.ecss.2019.106345

MacCready, P. (2004). Toward a unified theory of tidally-averaged estuarine salinity structure. *Estuaries*, *27*(4), 561–570. https://doi.org/10.1007/BF02907644

MacCready, P. (2007). Estuarine adjustment. *Journal of Physical Oceanography*, *37*(8), 2133–2145. https://doi.org/10.1175/JPO3082.1

Maicu, F., De Pascalis, F., Ferrarin, C., & Umgiesser, G. (2018). Hydrodynamics of the Po River-Delta-Sea system. *Journal of Geophysical Research: Oceans*, *123*(9), 6349–6372. https://doi.org/10.1029/2017JC013601

Qiu, C., & Zhu, J. (2015). Assessing the influence of sea level rise on salt transport processes and estuarine circulation in the Changjiang River Estuary. *Journal of Coastal Research*, *31*(3), 661–670. https://doi.org/10.2112/JCOASTRES-D-13-00138.1

Ralston, D. K., & Geyer, W. R. (2019). Response to channel deepening of the salinity intrusion, estuarine circulation, and stratification in an urbanized estuary. *Journal of Geophysical Research: Oceans*, *124*(7), 4784–4802. https://doi.org/10.1029/2019JC015006

Ralston, D. K., Geyer, W. R., & Lerczak, J. A. (2008). Subtidal salinity and velocity in the Hudson River estuary: Observations and modeling. *Journal of Physical Oceanography*, *38*(4), 753–770. https://doi.org/10.1175/2007JPO3808.1

Wang, B., Zhu, J., Wu, H., Yu, F., & Song, X. (2012). Dynamics of saltwater intrusion in the Modaomen Waterway of the Pearl River Estuary. *Science China Earth Sciences*, *55*(11), 1901–1918. https://doi.org/10.1007/s11430-012-4371-x

Wang, J., de Swart, H. E., & Dijkstra, Y. M. (2021). Dependence of tides and river water transport in an estuarine network on river discharge, tidal forcing, geometry and sea level rise. *Continental Shelf Research*, *225*, 104476. https://doi.org/10.1016/j.csr.2021.104476

Wu, H., Zhu, J., Chen, B., & Chen, Y. (2006). Quantitative relationship of runoff and tide to saltwater spilling over from the North Branch in the Changjiang Estuary: A numerical study. *Estuarine, Coastal and Shelf Science*, *69*(1–2), 125–132. https://doi.org/10.1016/j.ecss.2006.04.009

Wu, H., Zhu, J., & Ho Choi, B. (2010). Links between saltwater intrusion and subtidal circulation in the Changjiang Estuary: A model-guided study. *Continental Shelf Research*, *30*(17), 1891–1905. https://doi.org/10.1016/j.csr.2010.09.001

Xue, P., Chen, C., Ding, P., Beardsley, R. C., Lin, H., Ge, J., & Kong, Y. (2009). Saltwater intrusion into the Changjiang River: A model-guided mechanism study. *Journal of Geophysical Research*, *114*(C2), C02006. https://doi.org/10.1029/2008JC004831

Zhang, M., Townend, I., Zhou, Y., & Cai, H. (2016). Seasonal variation of river and tide energy in the Yangtze estuary, China. *Earth Surface Processes and Landforms*, *41*(1), 98–116. https://doi.org/10.1002/esp.3790

Zhu, J., Ding, P., Zhang, L., Wu, H., & Cao, H. (2006). Influence of the deep waterway project on the Changjiang Estuary. In *The environment in Asia Pacific harbours* (pp. 79–92). Springer. https://doi.org/10.1007/1-4020-3655-8_6

Zhu, J., Weisberg, R. H., Zheng, L., & Han, S. (2015). Influences of channel deepening and widening on the tidal and nontidal circulations of Tampa Bay. *Estuaries and Coasts*, *38*(1), 132–150. https://doi.org/10.1007/s12237-014-9815-4

Zhu, J., Wu, H., Li, L., & Qiu, C. (2018). Saltwater intrusion in the Changjiang Estuary. In X. S. Liang & Y. Zhang (Eds.), *Coastal environment, disaster, and infrastructure - A case study of China's coastline* (pp. 49–73). IntechOpen. https://doi.org/10.5772/intechopen.80903

Zhu, L., Gong, W., Zhang, H., Yuan, L., Hu, S., & Li, S. (2021). Determining the subtidal flow at a stratified tidal junction by a novel repeated measurements method. *Applied Ocean Research*, *113*, 102738. https://doi.org/10.1016/j.apor.2021.102738

Zimmerman, J. (1986). The tidal whirlpool: A review of horizontal dispersion by tidal and residual currents. *Netherlands Journal of Sea Research*, *20*(2–3), 133–154. https://doi.org/10.1016/0077-7579(86)90037-2